Two crossover regions in the dynamics of glass forming epoxy resins

S. Corezzi
INFM and Dipartimento di Fisica, Università di Perugia, 06123 Perugia, Italy

M. Beiner, H. Huth, and K. Schröter
Fachbereich Physik, Universität Halle, 06099 Halle (Saale), Germany

S. Capaccioli and R. Casalini
INFM and Dipartimento di Fisica E. Fermi, Università di Pisa, 56127 Pisa, Italy

D. Fioretto[a)]
INFM and Dipartimento di Fisica, Università di Perugia, 06123 Perugia, Italy

E. Donth
Fachbereich Physik, Universität Halle, 06099 Halle (Saale), Germany

(Received 27 September 2001; accepted 25 April 2002)

Broadband dielectric spectroscopy, heat capacity spectroscopy (3ω method), and viscosimetry have been used to study the dynamic glass transition of two glass-forming epoxy resins, poly [(phenyl glycidyl ether)-*co*-formaldehyde] and diglycidyl ether of bisphenol-*A*. In spite of their rather simple molecular structure, the dynamics of these systems is characterized by two well-separated crossover regions where the relaxation times of main transition and the two secondary relaxations β and γ approach each other. The main transition has three parts: The a process at high temperature, the a' process between the two crossover regions, and the α process at low temperatures. Both the γ-crossover region [around a temperature $T_c(\gamma)\sim(1.4-1.5)T_g$ and a relaxation time $\tau_c(\gamma)\approx 10^{-10}$ s] and the β-crossover region [around $T_c(\beta)\sim(1.1-1.2)T_g$ and $\tau_c(\beta)\approx 10^{-6}$ s] could be studied within the experimentally accessible frequency–temperature window. Different typical crossover properties are observed in the two regions. The γ-crossover region is characterized by onset of the (a',α) process, with a relaxation time about one decade greater than that of the quasicontinuous (a,γ) trace. The β-crossover region is characterized, besides splitting of main andβ relaxation times, by a change in the temperature dependence of the main-relaxation time as reflected by a bend in the Stickel plot of the continuous (a',α) trace, the separation of individual temperature dependences of different transport properties such as impurity-ions diffusion coefficient and viscosity, and a temperature-dependent main relaxation time that starts to be in accordance (at lower temperatures) with the Adam–Gibbs model. The cooperativity of the main process between the γ and β crossover seems to be small. Below the β crossover, cooperativity increases up to values of order $N_\alpha\sim 100$ near T_g, and configurational entropy seems to correlate with the main relaxation time. © *2002 American Institute of Physics.* [DOI: 10.1063/1.1486214]

I. INTRODUCTION

In condensed matter physics, increasing interest is devoted to the glass transition phenomenon. In this field, some common aspects in the dynamics of different systems suggest that, despite material-specific aspects, some common basic interpretation should be found for the liquid to glass transition. In particular, it is well known that various glasses from small molecules to polymers show a relatively similar relaxation map (i.e., temperature dependence of the characteristic times), with a main dynamic transition (a and α process) whose characteristic time tends to diverge close to the conventional glass transition temperature T_g, and one or more secondary processes (β, γ, ...) that persist also below T_g. In the last few years an increasing number of crossover effects along the trace of the main dynamic transition has been reported for several liquids. In these studies, concerned with systems with only one secondary relaxation, the crossover effects usually occur in a narrow frequency–temperature range, a marked region in the Arrhenius diagram above T_g generally called the crossover region. This region can be characterized (see, e.g., Refs. 1 and 2) by several properties:

(i) Splitting of the high-temperature process (a) into the cooperative α process and the local secondary process,[3–6] as seen from above, or merging of the α and secondary process into the a process, as seen from below.

(ii) Extrapolated onset of the dielectric and calorimetric intensity of the α process [i.e., $\Delta\varepsilon_\alpha\to 0$, $\Delta c_{p,\alpha}\to 0$ (Refs. 7–9)] for scenario I (see below).

(iii) Bend in the trace of the main (a,α) transition, known as Stickel bend,[10–13] corresponding to a change, within a small temperature interval, of the Vogel–Fulcher–Tamman parameters for the a process to different parameters for the α process. The Vogel temperature T_0 for the α pro-

a)Author to whom correspondence should be addressed. Email address: daniele.fioretto@pg.infn.it

cess is, as a rule (scenario II, see below), smaller than the Vogel temperature for the *a* process, i.e., $T_0(\alpha) < T_0(a)$.

(iv) Separation of the individual temperature dependences of different transport properties such as self-diffusion and viscosity.[14–16] This is connected with the *breakdown* of the Stokes–Einstein law of diffusion.[17]

(v) The plot of the logarithm of the characteristic time for the main transition versus the reciprocal configurational entropy (more precisely, versus $1/TS_c$), inspired by the Adam–Gibbs relation,[18] shows a bend.[19]

By proper extrapolations, characteristic crossover temperatures for the above-mentioned effects are found to range within a temperature interval of about 10 K.[1,20] For the sake of brevity, we will refer to the crossover temperature as an average temperature value of the crossover region. For fragile glass-formers a typical crossover temperature T_c is about $T_c \approx 1.2T_g$. The corresponding relaxation time region in the Arrhenius diagram is typically around $\tau_c \approx 10^{-6}$ s. However, both values (τ_c and T_c/T_g) show a large variance in groups of different substances, as discussed in Refs. 1 and 21. We know also a series of substances where T_c tends systematically to the glass transition temperature, $T_c \rightarrow T_g$: the poly(*n*-alkyl methacrylate)s, where T_g is reached near the hexyl member.[22]

As recalled at point (i), crossover effects are often accompanied by the occurrence of a splitting phenomenon, i.e., separation of the relaxation times of dynamic glass transition and a secondary relaxation. In a rough, preliminary classification we can recognize two scenarios of the crossover region[7,23,24] (see also Refs. 25–27) in connection with the type of splitting region:

Scenario I. Separate onset of the α process about one to two frequency decades (frequency gap) below the continuous trace of the *a* and β processes. This last trace shows there a more or less pronounced bend in the Arrhenius diagram. The crossover region can be defined by the extrapolation to zero of the α intensity.

Scenario II. A continuous trace of the main (a,α) transition where the crossover region can be defined by the extrapolation from low temperatures of the trace of the β process, running into the main process with a large ''angle'' in the Arrhenius diagram and with a usually small relaxation intensity [e.g., $\Delta\varepsilon_\beta \ll (\Delta\varepsilon_a, \Delta\varepsilon_\alpha)$ near T_c].

It was speculated[24] that the molecular cage for the *a* process is larger for scenario II than for scenario I, inducing for scenario II ''more continuity'' between the *a* process and the cooperative α process, with increasing size of the cooperativity regions below the crossover.[28]

The aim of the present paper is the experimental study of the dynamic glass transition in two epoxy resins: poly[(phenyl glycidyl ether)-co-formaldehyde] (PPGE) and diglycidyl ether of bisphenol-*A* (DGEBA). The main interest for these systems is that they both show two secondary relaxations that approach the main transition inside the experimentally accessible frequency window. Following the tradition of polymer physics, the secondary relaxation at lower frequencies is called the β process, and that at higher frequency is called the γ process. We use the term *crossover region* to indicate a temperature–frequency region where changes take place in the dynamic behavior of the system. From broadband dielectric spectroscopy we have indication of two well-separated crossover regions (β crossover and γ crossover), with $\tau_c(\beta) \approx 10^{-6}$ s and $\tau_c(\gamma) \approx 10^{-10}$ s. We use additionally viscosity measurements and heat capacity spectroscopy (3ω method) to study the following two questions:

(A) Which property (ii)–(v) can be observed in the two different crossover regions (β crossover and γ crossover)? Especially, can the two crossover regions also be classified within scenario I or scenario II?

(B) What is the character of the part of the main transition between the two crossovers? Especially, is it more a high-temperature process (similar to the *a* process, therefore called a'), or is it more a cooperative process (similar to the α process, hence the name α')?

The results for our low-molecular-weight epoxy resins will be finally compared with dielectric measurements from literature on other substances with two secondary relaxations.

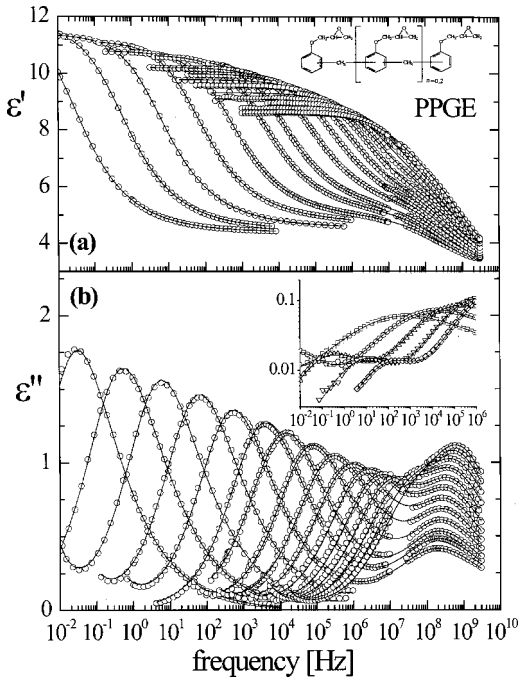

FIG. 1. (a) Real and (b) imaginary part of the complex dielectric constant $\varepsilon^*(\omega)$ for PPGE (selected data) at several temperatures (331.8, 327.9, 323.1, 317.9, 313.0, 308.0, 303.1, 298.3, 293.1, 287.5, 283.9, 278.9, 274.4, 270.1, 266.3, 262.1 K) above T_g, in the range 10^{-2}–3×10^9 Hz. The solid lines represent a fit with two HN functions. In the inset: dielectric loss at some temperatures (213, 193, 173, 153, 133 K) below T_g, showing the γ process and the less intense β process. The best fit with a symmetrical Cole–Cole function plus a HN function is shown by solid lines.

II. EXPERIMENT

A. Samples

The sample of DGEBA used in this study was purchased from Shell Co. under the trade name of Epon 828 [average molecular weight ~380 g/mol, corresponding to $n \sim 0.14$ in the chemical formula reported in Fig. 1(a)]. It is a widely used commercial epoxy resin, and was measured as pur-

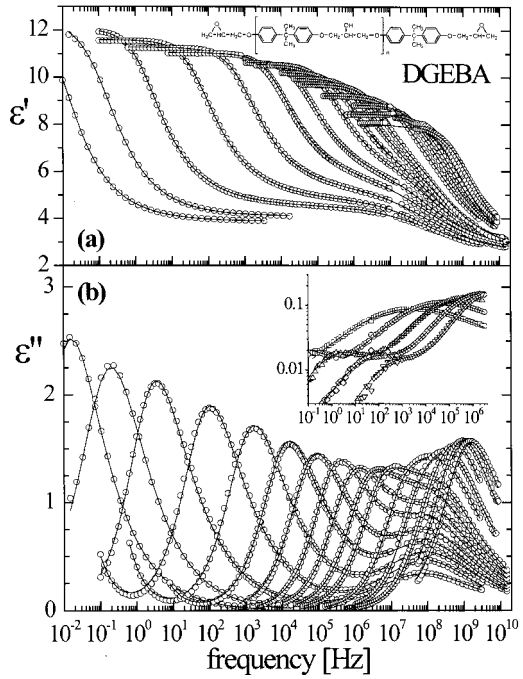

FIG. 2. (a) Real and (b) imaginary part of $\varepsilon^*(\omega)$ for DGEBA (selected data) at several temperatures (353, 343, 333, 323, 313, 303, 298, 293, 288, 283, 278, 273, 268, 263, 259, 256 K) above T_g, in the range 10^{-2}–2×10^{10} Hz. The solid lines represent a fit with two HN functions. In the inset: dielectric loss at some temperatures (223, 203, 183, 163, 143 K) below T_g, showing the γ process at higher frequencies and the β process at lower frequencies. The best fit with a symmetrical Cole–Cole function plus a HN function is shown by solid lines.

chased. PPGE is an epoxy resin with average molecular weight of 345 g/mol. It was obtained from Aldrich Chemicals and was measured as received. The chemical formula of this material is given in Fig. 2(a). The conventional glass transition temperatures are $T_g=255\pm1$ K for DGEBA and $T_g=258\pm1$ K for PPGE. The T_g values were obtained by an equal-area construction from differential scanning calorimetry (DSC) curves, acquired by a Perkin-Elmer DSC 7 apparatus, at a heating rate of $dT/dt=+10$ K/min.

B. Measurements

1. Dielectric spectroscopy

Due to the strong permanent dipoles originating from the presence of epoxy groups (~2.1 D per epoxy group), both DGEBA and PPGE are particularly suitable for a dielectric investigation. Measurements of the dielectric constant $\varepsilon^*(\omega,T)=\varepsilon'-i\varepsilon''$ in PPGE were carried out by means of an Alpha Novocontrol dielectric analyzer (Pisa & Mainz) and an impedance analyzer HP4194A (Pisa) in the frequency range from 10^{-2} to 10^7 Hz. A network analyzer HP8753A (Perugia) was used to cover the frequency range from 10^7 to 3×10^9 Hz. Isothermal frequency scans were performed in the temperature interval from 357.8 to 133.2 K, during several series of measurements.

The dielectric constant of DGEBA was measured in the frequency range from 10^{-1} to 10^6 Hz by a Novocontrol BDS 4000 based on a Solartron FRA 1260 (Halle). The temperature interval was from 123.2 to 293.2 K, i.e., from far below to well above the glass transition temperature, in steps of 5 degrees. The results are compared with previously published dielectric data in the frequency range from 10^2 to 2×10^{10} Hz (Ref. 8) and data at lower frequencies down to 10^{-2} Hz (Ref. 29). Altogether we present dielectric results for DGEBA covering 12 decades of frequency, obtained in the temperature range from 123.2 to 353.2 K.

The real and imaginary parts of the dielectric constant, $\varepsilon'(\omega)$ and $\varepsilon''(\omega)$, of our samples are displayed in Figs. 1 and 2 at several temperatures. The isothermal data for the dielectric constant were analyzed in terms of linear superposition of relaxation and conductivity contributions (*additive ansatz*), with each relaxation process described by a Havriliak–Negami (HN) function:

$$\varepsilon^*(\omega)-\varepsilon_\infty=\sum_k \frac{\Delta\varepsilon_k}{[1+(i\omega\tau_{HN_k})^{1-\alpha_k}]^{\beta_k}}-\frac{i\sigma}{\omega\varepsilon_0}. \tag{1}$$

In Eq. (1) the index k runs over the relaxation processes and the conductivity effect is taken into account by the term $-i\sigma/\omega\varepsilon_0$ (ε_0 is the dielectric permittivity of vacuum). ε_∞ is the high-frequency limit of ε' outside the dispersion zone, and $\Delta\varepsilon_k$ is the dielectric strength of each process. The fit with this phenomenological function allows us to extract characteristic parameters for the different relaxation peaks, i.e., the frequency of maximum loss and the peak shape. The frequency of maximum ε'', f_{max}, can be analytically calculated from the HN fitting parameters by

$$f_{max}=(2\pi\tau_{HN})^{-1}\sin^{1/(1-\alpha)}\left(\frac{\pi(1-\alpha)}{2(1+\beta)}\right)\sin^{-1/(1-\alpha)}\times\left(\frac{\pi(1-\alpha)\beta}{2(1+\beta)}\right). \tag{2}$$

From this quantity a characteristic relaxation time $\tau_{max}=(2\pi f_{max})^{-1}$, can be easily obtained, usually preferred to τ_{HN} since it is a model-independent parameter. Concerning the shape of the dielectric peak, the HN function gives the asymptotic behavior of $\varepsilon''(\omega)$ in the low- and high-frequency limits as power laws, $\varepsilon''\propto\omega^m$ and $\varepsilon''\propto\omega^{-n}$ respectively, whose exponents are simply expressed in terms of the HN shape parameters α and β through the relations $m=(1-\alpha)$ and $n=\beta(1-\alpha)$.

The real and the imaginary parts of $\varepsilon^*(\omega)$ have been fitted simultaneously by using the nonlinear least-squares Levenberg–Marquard routine. The uncertainties of the fitting parameters have been estimated by means of a Monte Carlo procedure. In particular, starting from each experimental spectrum 100 ''artificial'' data sets have been produced by means of the bootstrap Monte Carlo method,[30] replacing a random fraction of original points by duplicated original points. Each data set has been fitted by means of the Levenberg–Marquardt routine, giving a distribution of fitting parameters. An estimate of the error of each parameter has been obtained by the standard deviation of the probability distribution of the fitting parameters. Finally, the errors of the HN fitting parameters have been used to estimate the error of the relaxation time τ_{max}.

2. Heat capacity spectroscopy (HCS)

The dynamic effusivity $\rho\kappa c_p^*(\omega,T)=\rho\kappa c_p'-i\rho\kappa c_p''$ (κ is the heat conductivity, ρ the density, and c_p^* the dynamic heat capacity) was measured by the 3ω method[31] in the frequency range from 0.2 to 2000 Hz. Nickel heaters with a thickness of about 70 nm on poly(ether ether ketone) (PEEK) substrates were used. The temperature coefficient of resistance was about 2000 ppm/K. The nickel heater was placed in a Wheatstone bridge that was equilibrated automatically during the measurements. The remaining difference signal across the bridge was preamplified by a low-noise preamplifier (EG&G 5113). A 12-bit analog to digital converter was used to collect the data. Amplitude and phase of the third harmonic were determined afterwards by a selective Fourier transformation. Further experimental details about our setup are described elsewhere.[32,33]

Measurements on two different heaters were performed for both epoxy samples: small nickel heaters ($1.5\times 6\ \mathrm{mm}^2$) were used for high frequencies (>1 Hz), large nickel heaters ($5\times 10\ \mathrm{mm}^2$) were used for low frequencies (0.2–20 Hz). This ensures the signal amplitude and precision to be large enough at high frequencies (amplitude $\sim\omega^{-1/2}$) and the thermal wavelength to be small compared to the heater dimensions at low frequencies as required by the data evaluation concept. The samples were equilibrated for 30 min before an isothermal frequency sweep was started

The frequency-dependent width of the α peak, δT, and the dynamic glass transition temperature, T_ω, were determined by Gaussian fits to the isochronal ($\omega=$const) data for the imaginary part $\rho\kappa c_p''(T)$. The calorimetric α intensity was obtained from a tangent construction to the real part $\rho\kappa c_p'(T)$ [see Fig. 3(c)]. To get finally $\Delta(1/c_p)$ values from our 3ω method output, the data were adjusted to heat capacities c_p^* from temperature-modulated DSC (TMDSC) at $\omega=2\pi/60$ s. A fixed factor correction was used: all isochrones of one 3ω run were divided by a heater-specific mean value of $\rho\kappa$. The error caused by this temperature- and frequency-independent mean value $\rho\kappa$ correction is found to be small.[34] The isochronal HCS sweeps of Fig. 3 are transferred into isothermal $\rho\kappa c_p^*$ data versus frequency in Fig. 4.

3. Viscosity measurements

The shear viscosity was measured with a Rheometrics Dynamic Analyzer RDA-II and a Dynamic Stress Rheometer DSR instruments from Rheometrics Scientific in plate-plate geometry. Parallel plates with a diameter of 25 mm were used in the temperature range from 276 to 379 K for PPGE and in the range from 269 to 339 K for DGEBA. The sample thickness was about 1.5 mm. A shear rate sweep over one decade was performed at each temperature to prove the Newtonian behavior of the liquid. The thermal expansion of the tools (about 2.5 μm/K) and the samples was corrected during the measurements. Some data points at temperatures between 267 and 259 K were added for DGEBA by extending the sample between two 8 mm plates to a hyperboloid with a final length of about 8 mm (for details see Ref. 35). In the temperature range from 332 to 453 K viscosity was measured by an Ubbelohde type viscosimeter ($k=0.05\ \mathrm{mm}^2/\mathrm{s}^2$). An oil bath was used to control the sample temperature. The viscosity was calculated according to $\eta=t_U k\rho$ from flow time t_U, capillary constant k, and temperature-dependent density ρ. The density $\rho(T)=\rho_0[1-\alpha_V(T-273)]$) for DGEBA was measured by a Guy–Lussac-type picnometer at temperatures between 296 and 318 K and extrapolated to higher temperatures. A thermal

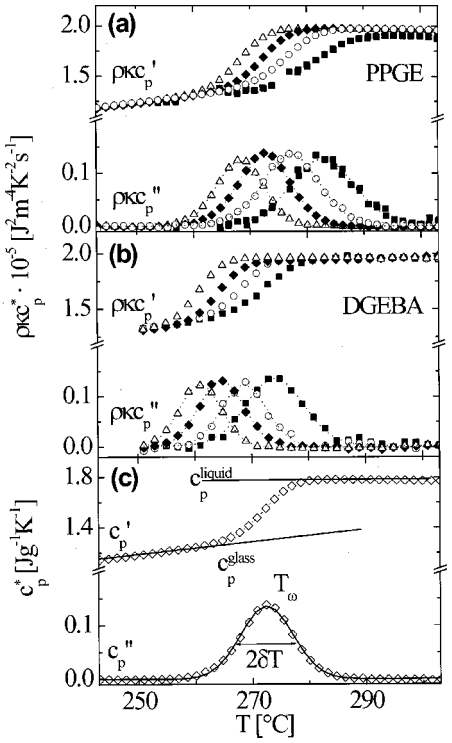

FIG. 3. Real and imaginary parts of the HCS signal, $\rho\kappa c_p^*$, as a function of temperature for (a) PPGE and (b) DGEBA (2 Hz, triangle; 20 Hz, diamond; 200 Hz, circle; 2 kHz, square). The method of determining the calorimetric parameters T_ω and δT from a Gaussian fit to the imaginary part and $\Delta(1/\rho\kappa c_p)$ from a tangent construction to the real part is shown in part (c), where isochronal data at 20 Hz for PPGE are used.

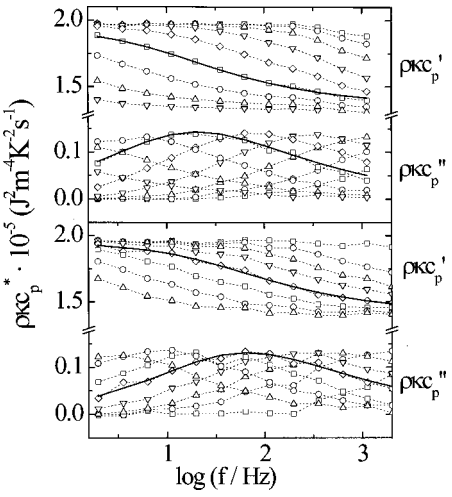

FIG. 4. Real and imaginary parts of $\rho\kappa c_p^*$ as a function of frequency for PPGE (upper frame) and DGEBA (lower frame). The solid lines show an example of a HN fit to the data (corresponding to $T=274$ K for PPGE, and $T=269.1$ K for DGEBA). The dashed lines are only guides to the eyes.

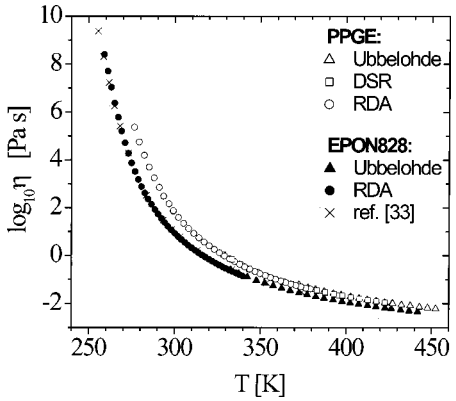

FIG. 5. Logarithm of viscosity vs temperature for PPGE and DGEBA, obtained by different devices as explained in the legend.

expansion coefficient $\alpha_V=(6.26\pm0.03)\times10^{-4}$ K^{-1} and a density at 273 K $\rho_0=1.1823\pm0.0003$ g/cm^3 were obtained for DGEBA. The corresponding values for PPGE taken from measurements in the range from 287 to 332 K were $\alpha_V=(6.3\pm0.1)\times10^{-4}$ K^{-1} and $\rho_0=1.2266\pm0.0003$ g/cm^3.

Figure 5 shows the viscosity data for DGEBA and PPGE over the whole temperature range measured. For comparison, the same figure includes some viscosity data for DGEBA from dynamical mechanical measurements, carried out via a Rheometrics RMS 800 in the range from 255 to 374 K and published in a previous article[36] where experimental details can also be found.

III. RESULTS

The isothermal dielectric spectra of PPGE and DGEBA (Figs. 1 and 2) show clearly the presence of two relaxation processes for $T>T_g$: the main (α) process and a secondary (γ) process. As the temperature increases above T_g, the α relaxation shifts toward higher frequencies, approaching the secondary peak in the GHz region. For $T<T_g$ the main relaxation is out of the accessible frequency window, and it is possible to identify a further very small secondary (β) process whose loss peak position is intermediate between the α and γ processes [see inset in Figs. 1(b) and 2(b)]. Concerning the spectral shape, both the main and secondary relaxations of PPGE and DGEBA show a pronounced non-Debye character [i.e., $\beta\neq1$ and/or $\alpha\neq0$ in Eq. (1)]; in particular, the β relaxation can be well represented by a symmetrical Cole–Cole function (i.e., $\beta=1$) with $\alpha\approx0.5$. The dielectric strength of the β relaxation is very small compared to that of the α relaxation (e.g., we find $\Delta\varepsilon_\beta$ below T_g to be around 0.05, that is about 1% of $\Delta\varepsilon_\alpha$, for both PPGE and DGEBA), so that we cannot follow its trace above T_g any more. In the present analysis we neglect its contribution and use the sum of two HN terms, one for the α and the other for the γ relaxation, to describe the spectra above T_g. The fitting curves are drawn as solid lines in Figs. 1 and 2, where the conductivity contribution has been cut off from the lower-frequency part of the spectra for reasons of clarity. Due to the progressive overlap of the α and γ relaxations, it becomes more and more difficult to obtain meaningful values for the shape parameters by increasing the temperature. We thus chose to fit the high-temperature ($T>303$ K) spectra of PPGE by constraining the shape of the α relaxation to vary within the range of values found at lower temperatures, where the time–temperature superposition principle appears to be well satisfied ($m_\alpha=0.64\pm0.02; n_\alpha=0.40\pm0.01$). In the case of DGEBA, the fit procedure of the spectra has been repeated by exploiting the data at lower frequencies and adopting at the highest temperatures ($T>288$ K) the criterion of keeping invariant the parameter $n_\alpha\sim0.4$ as found at lower temperature. This criterion was motivated by the time–temperature superposition principle and supported by previous light-scattering results[36] for the shape of the main process in DGEBA over the same temperature interval as the present dielectric investigation. In fact, the mutual consistency of dielectric and depolarized light-scattering shape parameters was observed, although the characteristic times of the process revealed by the two techniques were different. Since in case of light-scattering spectra there is no signature of the secondary peak visible in the dielectric ones, a more reliable determination of the α shape parameters could be made, giving $m_\alpha\sim0.9$ and $n_\alpha\sim0.4$.[36] In our dielectric fit procedure the shape parameter m_α was set as free; anyway, its value was found almost constant around 0.9 (see also Table I), thus validating the guess of a shape invariance. The parameters for the α relaxation of PPGE and DGEBA obtained from the HN fit at several temperatures are given in Table I with error estimates.

The isothermal HCS spectra of PPGE and DGEBA reported in Fig. 4 show a well-defined peak in the imaginary part $\rho\kappa c_p''(\omega)$, corresponding to the characteristic relaxation step in the real part $\rho\kappa c_p'(\omega)$. In the frequency and temperature range investigated here only one relaxation process is observed. In principle, all $\rho\kappa c_p^*$ isotherms could be approximated by a single HN function, giving for each temperature, after reduction by $\rho\kappa$, the frequency of maximum c_p'', the calorimetric α intensity Δc_p, and the shape parameters, in a manner similar to Eq. (1). However, several sources of error make the data $\rho\kappa c_p^*(\omega)$ subject to considerable uncertainty[32,37] and limit, together with the narrow frequency range accessible, the possibility for determining a reliable set of fit parameters. In the present case, only for a few temperatures can the whole set of HN fit parameters be determined with reasonable accuracy. In particular, the fit of $\rho\kappa c_p^*(\omega)$ for PPGE at 274 K results in $\Delta(\rho\kappa c_p)=(5.96\pm0.30)\times10^{-4}$ J^2 cm^{-4} K^{-2} s^{-1}, $\tau_{HN}=(6.7\pm1.9)\times10^{-3}$ s, $m=0.68\pm0.04$, and $n=0.44\pm0.07$, while the fit of $\rho\kappa c_p^*(\omega)$ for DGEBA at 269.1 K gives $\Delta(\rho\kappa c_p)=(5.37\pm0.55)\times10^{-4}$ J^2 cm^{-4} K^{-2} s^{-1}, $\tau_{HN}=(1.67\pm0.09)\times10^{-3}$ s, $m=0.67\pm0.06$, and $n=0.39\pm0.11$. The corresponding fitting curves are reported as solid lines in Fig. 4. For each system, the data at all other temperatures were fitted by fixing the shape parameters within the range allowed by these values. The results for Δc_p and τ_{max} are in fair agreement with those obtained in the corresponding temperature range from tangent construction and Gaussian fits to isochronal data. We note that shape parameters obtained by HCS are not far away from those obtained by dielectric spectroscopy. Usually it is found[31,37–39] that c_p'' peaks tend to be narrower and more symmetric than the corresponding dielectric loss curves.

TABLE I. Havriliak–Negami fit parameters for the α relaxation of PPGE and DGEBA at several temperatures. When a shape parameter was undergoing additional constraints as explained in the text, the respective error is not reported.

PPGE					DGEBA				
T (K)	τ_{HN} (s)	m_α	n_α	$\Delta\varepsilon_\alpha$	T (K)	τ_{HN} (s)	m_α	n_α	$\Delta\varepsilon_\alpha$
331.8	$(7.6\pm3)\times10^{-9}$	0.63	0.41	2.7±0.6	343	$(9.5\pm2.3)\times10^{-10}$	1±0.03	0.42	0.6±0.3
327.9	$(1.04\pm0.06)\times10^{-8}$	0.63	0.40	3.1±0.6	333	$(2.4\pm0.5)\times10^{-9}$	1±0.03	0.42	1.3±0.2
323.1	$(1.80\pm0.05)\times10^{-8}$	0.64	0.40	3.2±0.3	323	$(5.0\pm0.5)\times10^{-9}$	1±0.04	0.42	2.0±0.3
317.9	$(3.6\pm0.2)\times10^{-8}$	0.63	0.40	3.4±0.4	313	$(1.25\pm0.08)\times10^{-8}$	0.95±0.03	0.41	2.7±0.2
313.0	$(6.6\pm0.2)\times10^{-8}$	0.63	0.40	3.8±0.3	303	$(4.48\pm0.13)\times10^{-8}$	0.88±0.02	0.41	3.5±0.4
308.0	$(1.45\pm0.06)\times10^{-7}$	0.63	0.39	4.1±0.4	298	$(1.08\pm0.05)\times10^{-7}$	0.87±0.02	0.41	3.9±0.5
303.1	$(3.8\pm0.2)\times10^{-7}$	0.61±0.02	0.39±0.02	4.4±0.2	293	$(3.21\pm0.08)\times10^{-7}$	0.88±0.02	0.39	4.2±0.3
298.3	$(1.07\pm0.03)\times10^{-6}$	0.62±0.02	0.39±0.02	4.7±0.3	288	$(8.9\pm0.4)\times10^{-7}$	0.86±0.03	0.40±0.05	4.7±0.3
293.1	$(4.13\pm0.06)\times10^{-6}$	0.64±0.015	0.39±0.02	4.9±0.2	283	$(3.75\pm0.12)\times10^{-6}$	0.86±0.03	0.40±0.04	5.1±0.3
287.5	$(2.190\pm0.013)\times10^{-5}$	0.63±0.02	0.39±0.02	5.39±0.15	278	$(2.21\pm0.06)\times10^{-5}$	0.83±0.02	0.39±0.02	5.71±0.03
283.9	$(7.8\pm0.3)\times10^{-5}$	0.64±0.02	0.40±0.02	5.6±0.2	273	$(2.12\pm0.08)\times10^{-4}$	0.85±0.01	0.40±0.01	6.21±0.03
278.9	$(5.7\pm0.2)\times10^{-4}$	0.65±0.01	0.40±0.01	5.9±0.2	268	$(3.39\pm0.09)\times10^{-3}$	0.85±0.01	0.40±0.01	6.83±0.05
274.4	$(4.82\pm0.13)\times10^{-3}$	0.65±0.01	0.40±0.01	6.38±0.05	263	$(7.1\pm0.3)\times10^{-2}$	0.82±0.02	0.43±0.02	7.37±0.05
270.1	$(5.22\pm0.17)\times10^{-2}$	0.65±0.01	0.39±0.01	6.8±0.2	261	$(3.2\pm0.2)\times10^{-1}$	0.82±0.02	0.43±0.02	7.73±0.08
266.3	$(5.7\pm0.1)\times10^{-1}$	0.65±0.02	0.40±0.01	7.2±0.2	259	$(1.65\pm0.04)\times1^{0}$	0.83±0.02	0.40±0.01	7.8±0.2
262.1	$(1.02\pm0.08)\times10^{1}$	0.67±0.03	0.40±0.01	7.5±0.2	256	$(2.25\pm0.06)\times10^{1}$	0.82±0.04	0.40±0.01	8.0±0.2

However, the significant uncertainty of HCS parameters restrains us from going into a deeper comparison.

The dielectric relaxation times τ_{max} obtained from the fitting procedure, together with the calorimetric characteristic times τ_{max} obtained from the location of the peak in the isochronal or isothermal $\rho\kappa c_p''$ spectra, are reported in the Arrhenius plot of Figs. 6 and 7 and compared with the viscosity data. The α trace of calorimetry and dielectrics coincide within the experimental uncertainty, and their temperature dependence closely parallels that of η. Figure 8 shows a convincing check of the relation $\tau_{max}\propto\eta$ in our samples, up to 332 K in PPGE and 343 K in DGEBA. It displays that a linear fit of log τ_{max} vs log η has slope 0.99±0.02 and 0.98 ±0.02 in PPGE and DGEBA, respectively. According to $\tau_{max}\propto\eta$, the viscosity data are rescaled up to the highest temperatures measured, and shown as solid lines in the Arrhenius plot of Figs. 6(a) and 7(a). We notice that the proportionality of τ_{max} to η in supercooled liquids has a physical basis in the α-scale universality predicted by the mode coupling theory and verified in different systems (e.g., see Ref. 40), but it is possible that at sufficiently high temperatures a $\tau_{max}\propto\eta/T$ regime ensues, as predicted by the hydrodynamic Debye model and recently observed in low-molecular-weight organic compounds.[13] However, the possible differences in Figs. 6 and 7 due to a $\eta\propto\tau_{max}T$ rescaling of the viscosity data for temperatures higher than those represented in Fig. 8 have no significant effect on the analysis and discussion reported in the following.

Together with the secondary relaxation times, Figs. 6(a) and 7(a) give the complete relaxation map of our samples in the supercooled and glassy state, as revealed by dielectric spectroscopy, HCS, and viscosity measurements. As known, the glass transition phenomenon is commonly described as an ergodic- to nonergodic-state transition and T_g is defined as the temperature at which the ergodicity is broken on the ex-

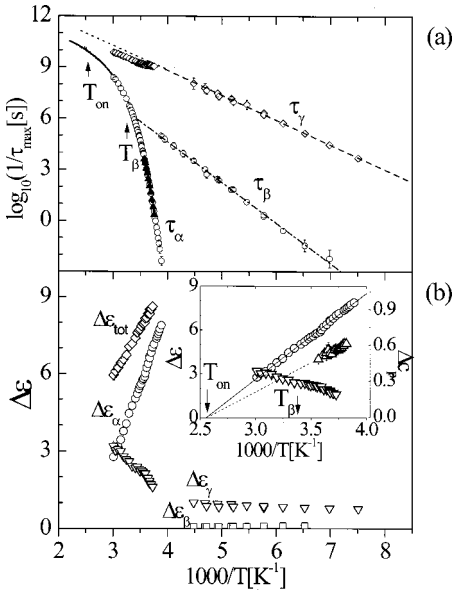

FIG. 6. (a) Arrhenius plot for PPGE. The temperature dependence of the dynamic glass transition is reconstructed via the trace of $\tau_{max}=(2\pi f_{max})^{-1}$ from ε'' (open circles) and $\rho\kappa c_p''$ (solid triangles), and via the viscosity data [the solid line shows experimental data of $\log(\kappa\eta^{-1})$, with $\log\kappa=8.3$ and η in Pa s]. The dielectric γ and β relaxation times are reported with diamond and squares, respectively. The dash line is an Arrhenius fit to the $T<T_g$ γ relaxation data [$\log\tau_0(s)=-14.7\pm0.2$, $E_a=6.67\pm0.15$ kcal/mol]; its extrapolation above T_g is drawn with dot line. The dash-dotted line is an Arrhenius fit to the β-relaxation data [$\log\tau_0(s)=-14.6\pm0.3$, $E_a=11.3\pm0.2$ kcal/mol]. The β- and γ-crossover regions are indicated by arrows. (b) Temperature dependence of the dielectric strengths of PPGE. The inset shows, in an enlarged scale, $\Delta\varepsilon_\alpha$ (circles) and $\Delta\varepsilon_\gamma$ (down triangles) above T_g, and the calorimetric α intensity Δc_p (up triangles, in units J kg^{-1} K^{-1}). The solid line is a linear fit to $\Delta\varepsilon_\alpha$, extrapolated to the onset temperature T_{on}. The dashed line is not a fit, but only a guide to the eyes, drawn to demonstrate the compatibility of the Δc_p trend with the dielectric onset. Error bars smaller than the symbol size are omitted.

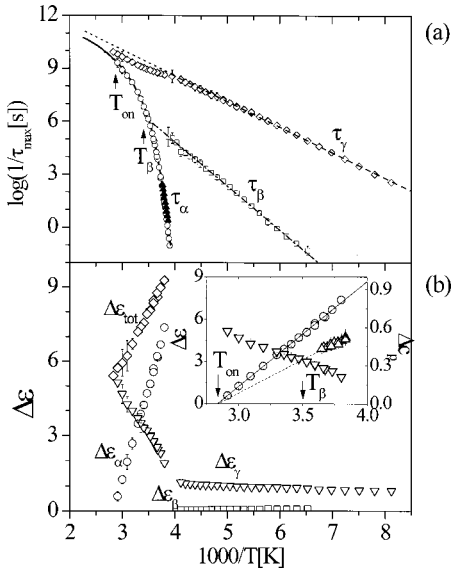

FIG. 7. (a) Arrhenius plot for DGEBA. The temperature dependence of the dynamic glass transition is reconstructed via the trace of $\tau_{max}=(2\pi f_{max})^{-1}$ from ε'' (open circles) and $\rho\kappa c_p''$ (solid triangles), and via the viscosity data (the solid line shows experimental data of $\log(\kappa\eta^{-1})$, with $\log\kappa=8.4$ and η in Pa s, also including data from Ref. 36). The dielectric γ- and β-relaxation times are reported with diamond and squares, respectively. The dashed line is an Arrhenius fit to the $T<T_g$ γ relaxation data [$\log\tau_0$ (s)$=-14.35\pm0.13$, $E_a=6.6\pm0.1$ kcal/mol]; its extrapolation above T_g is drawn with a dotted line. The dash-dotted line is an Arrhenius fit to the β relaxation data [$\log\tau_0$ (s)$=-14.78\pm0.09$, $E_a=11.38\pm0.08$ kcal/mol]. The β- and γ-crossover regions are indicated by arrows. (b) Temperature dependence of the dielectric strengths of DGEBA. The inset shows $\Delta\varepsilon_\alpha$ (circles) and $\Delta\varepsilon_\gamma$ (down triangles) above T_g, and the calorimetric α intensity Δc_p (up triangles, in units J kg^{-1} K^{-1}). The solid line is a linear fit to $\Delta\varepsilon_\alpha$, extrapolated to the onset temperature T_{on}. The dashed line is drawn as a guide to the eyes. Error bars smaller than the symbol size are omitted.

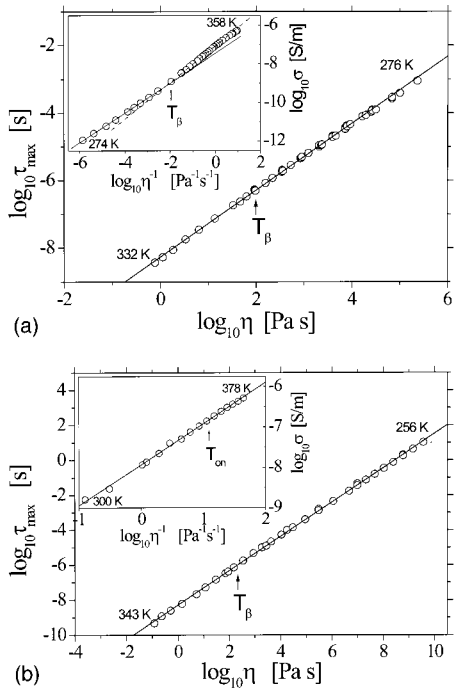

FIG. 8. Main frame: dielectric relaxation time τ_{max} vs viscosity η in a log–log representation, where the relation $\tau_{max}\propto\eta$ corresponds to a linear behavior with slope 1. (a) The solid line (slope 0.99 ± 0.02) is a linear fit to the data of PPGE over six decades, in the temperature range 276–332 K. (b) The straight line (slope 0.98 ± 0.02) is a linear fit to the data of DGEBA over ten decades, in the temperature range 256–343 K. Inset: Conductivity σ vs reciprocal viscosity η^{-1} in a log–log representation. The straight lines are fits of the relation $\sigma\eta^n=$const. (a) The fitting line corresponds to $n=0.77\pm0.03$ in the lower-temperature range (solid line) and $n=0.94\pm0.03$ in the higher-temperature range (dashed line) for PPGE, and (b) to $n=1.02\pm0.03$ in the temperature range 300–378 K for DGEBA. Data corresponding to characteristic temperatures are indicated (for the meaning of T_β and T_{on} see text).

perimental time scale. The characteristic time $\tau(T_g)$ may strongly depend on the experimental probe used and on the cooling rate; in particular, in a typical dielectric experiment the out-of-equilibrium state occurs when the structural relaxation time approximately exceeds 10^2 s. The dielectric value of T_g calculated in our samples by following this criterion is given in the second column of Table II, where good agreement with the calorimetric value from conventional DSC can be noticed. Also included in Table II is the steepness index $m=d(\log\tau)/d(T_g/T)|_{T=T_g}$, which quantifies the fragility of the system in terms of its temperature behavior at T_g.

At lower temperatures the system is in the nonequilibrium glassy state. There, two secondary processes (β and γ process) coexist, both showing Arrhenius behavior. The corresponding fitting parameters are listed in Table III. The dotted segment in Figs. 6(a) and 7(a) shows that at temperatures higher than T_g the γ trace deviates significantly from the extrapolation of the behavior below T_g. In particular, it first becomes flatter (i.e., lower apparent activation energy) and then goes on with increasing slope (i.e., increasing apparent activation energy), which becomes comparable to that found below T_g. Different approaches for analyzing relaxation functions in the case of the overlap of the two processes are debated in literature,[41–47] and their repercussions are especially expected in the Arrhenius diagram in the region where the processes tend to merge. Then we cannot completely rule out the possibility of some influence of the analysis method on the higher temperature τ_γ values. However, such an influence does not affect the data for the γ relaxation in the region where the separation from the α process is two decades at least, since under this condition an analysis of the $\alpha\gamma$ separation using the additive ansatz is always justified.[43,44,46] In particular, we notice that a deviation from the extrapolated Arrhenius behavior of the γ trace occurs just above T_g where the separation of the α and γ time scales is nearly ten decades, and this is actually confirmed by deconvoluting the α and γ processes according to alternative fitting procedures[48,49] based on the Williams ansatz.[41–47] Moreover, the effect of different fitting approaches on the relaxation time values at higher temperatures has been proven[48] not to affect qualitatively the trend of $\tau_\gamma(T)$, and we have no reason to think also the higher-temperature bending of the γ trace to be an artifact of the evaluation method.

Also the dc conductivity, σ, can be used as an efficient probe of the dynamics of supercooled systems. It should be noted that different samples of the same material might show different absolute σ values, since this is proportional to the amount of impurities in the sample (typically chlorine, in epoxy compounds). However, the temperature dependence of

TABLE II. Calorimetric and dielectric glass transition temperature, T_g, and temperatures used in identifying crossover effects in PPGE and DGEBA. The methods to determine T_B, T_β, and T_{on} are described in the text. T_{AG} is taken from Ref. 60. The frequency ω_β is defined as $\omega_\beta=\omega(T_\beta)$.

	T_g^{cal} (K)	T_g^{diel} (K)	m	T_B (K)	T_{AG} (K)	T_β (K)	$\log_{10}\omega_\beta$ (rad s^{-1})	$T_{on}(\Delta\varepsilon_\alpha\to 0)$ (K)	T_β/T_g^{cal}	T_{on}/T_g^{cal}
PPGE	258±1	258.4±0.5	~105	293±10	298	298±3	6.2	391±5	1.15±0.02	1.51±0.03
DGEBA	255±1	253.7±0.5	~95	275±10	288	285±3	6.1	351±4	1.12±0.02	1.38±0.02

σ is not affected by this problem, and a single curve can be obtained that is representative of the whole temperature behavior. The temperature dependence is expected to be closely related to that of viscosity. In particular, an inverse proportionality of σ to η would be expected in the hydrodynamic regime, though examples of supercooled liquids are not rare where a modified relation such as $\sigma\eta^n=$const holds, with $0<n<1$.[50] Actually, the inset of Fig. 8(b) shows that a simple proportionality is verified in DGEBA (at least above 306 K, where both conductivity and viscosity data are available for this system). In contrast, a single regime does not describe the data of PPGE [inset of Fig. 8(a)]. In this case the data in a log–log representation can be approximated by two straight lines, corresponding to $n=0.77$ at lower temperature and $n=0.94$ at higher temperature, crossing around 293–298 K.

The most traditional way of plotting relaxation times and viscosity and conductivity data as a function of temperature is the Arrhenius diagram, which magnifies the deviation from thermal activated behavior. On the other hand, a representation that goes into details of the temperature dependence and magnifies deviations from Vogel–Fulcher–Tamman (VFT) behavior at the same time is given by plotting the quantity $[d\log_{10}(1/x)/dT]^{-1/2}$ vs T, the so-called *Stickel plot*,[11] where x is the physical quantity usually reported in the Arrhenius diagram. In the Stickel plot a VFT behavior translates into a linear behavior. Figure 9 shows that a VFT regime extending over a wide temperature range can be certainly identified in both systems at higher temperature. At the same time it demonstrates a clear deviation of the lower-temperature data that could at first be approximated by a VFT equation with a different set of parameters. Since there is not a sharp but a continuous change in the trace of the data in the Stickel plot, a crossover temperature T_B can be identified with some difficulty: we located T_B where a bend starts in the higher temperature data, with a typical uncertainty of about ±10 K (see Table II). It should be noticed that intrinsic limits affect the Stickel procedure—it operates a shrinkage of several decades of dynamical data to a linear scale proportional to the temperature range, resulting in a smaller sensitivity for the low-temperature side, where a huge slowing down of the dynamics occurs in few tens of degrees—and different analytical strategies[39,51,52] can be adopted for testing the applicability of the VFT equation and for identifying changes in the temperature dependence of relaxation data.[53] It is found that the results for the lower-temperature range are mainly affected, where the validity itself of the VFT equation is questionable. Anyway, other procedures confirm the higher-temperature VFT regime in our data (the fitting curves for $T>T_B$ are reported in Fig. 9 as straight lines), but indicate a large variability in the set of VFT parameters describing the lower-temperature data (depending on the data range fitted) and a possible underestimation of T_B. The best VFT parameters obtained for τ_{max} and η in the high- and low-temperature regions separated by T_B are listed in Table III. We observe that the set of parameters in Table III fitting the data for $T<T_B$ also fit the data up to $\sim T_B+10$ K comparably well.

It must be noticed that in a previous investigation of DGEBA (see Fig. 5 of Ref. 50) we interpreted the small deviation of conductivity data from the linear behavior in the Stickel plot in a narrow temperature region (365–380 K) as the presence of a further deviation from a single VFT behavior. The possibility given here [Fig. 9(b)] of accessing much higher temperatures with viscosity data leads us to exclude the existence of such deviation and, within the experimental error, to identify a single VFT regime from T_B up to the highest temperatures.

A further source of information about crossover effects along the trace of the dynamic glass transition are the relaxation strengths. The fitting procedure of the dielectric spectra gives the strengths $\Delta\varepsilon$ of main and secondary relaxations as a function of temperature for PPGE and DGEBA, as reported in Figs. 6(b) and 7(b), respectively. They show very similar trends and comparable absolute values. Below the glass transition temperature, the β-relaxation strength $\Delta\varepsilon_\beta$ shows a very small value, systematically decreasing by increasing the temperature (by a factor of 3 over ~100 K). In contrast, the γ-relaxation strength $\Delta\varepsilon_\gamma$ shows a relatively small value, but systematically increases by increasing the temperature (by 50% over ~120 K). Above the glass transition temperature, the rate of increase of $\Delta\varepsilon_\gamma$ gets much higher, accompanied by a rapid decrease of the α-relaxation strength $\Delta\varepsilon_\alpha$. Figure 7(b) shows that in DGEBA $\Delta\varepsilon_\alpha$ really becomes very small and linearly extrapolates to zero at a finite onset temperature ($\Delta\varepsilon_\alpha\to 0$ for $T\to T_{on}$). In the case of PPGE the data do not give direct access to the α onset region, and a larger extrapolation of the linear fit [solid line in Fig. 6(b)] is needed to locate T_{on}.

We end this section by introducing an additional indicator of dynamic crossovers that we have considered in the present study, the cooperativity N_α, which is the number of particles per cooperatively rearranging region[18,24] (CRR). Calorimetric parameters from HCS are used to calculate N_α as the ratio between the volume of a CRR, $V_\alpha=\xi_\alpha^3$, and the mean volume of one molecule, according to a Nyquist-type fluctuation formula[54–56] derived in the von Laue approach to thermodynamics:[57]

$$N_\alpha=RT^2\Delta(1/c_v)/M_0\delta T^2\approx RT^2\Delta(1/c_p)/M_0\delta T^2. \quad (3)$$

TABLE III. Parameters of Arrhenius fit, $\tau(T)=\tau_0\exp(E_a/RT)$, to β and γ secondary relaxation times, and of VFT fit, $x(T)=x_0\exp[B/(T-T_0)]$, to main relaxation time ($x\equiv\tau_{\max}$, from dielectric spectroscopy) and viscosity ($\chi\equiv\eta$).

	Secondary relaxations				Main relaxation							
	γ relax. ($T<T_g$)		β relax. ($T<T_g$)		$\tau_{\max}$ ($T>T_B$ or T_β)			η ($T>T_B$ or T_β)			$\tau_{\max}$ ($T<T_B$ or T_β)	
	E_a (kcal mol^{-1})	log τ_0 (s)	E_a (kcal mol^{-1})	log τ_0 (s)	log τ_0 (s)	B (K)	T_0 (K)	log η_0 (Pa s)	B (K)	T_0 (K)	log τ_0 (s)	B (K)	T_0 (K)
PPGE	6.67±0.15	−14.7±0.2	11.3±0.2	−14.6±0.3	−12.2±0.1	800±30	240±1	−3.83±0.01	784±7	239.7±0.4	−15.7±0.2	181±60	204±1
DGEBA	6.6±0.1	−14.35±0.13	11.38±0.08	−14.78±0.09	−12.2±0.1	720±20	234.4±0.8	−3.80±0.02	717±6	234.2±0.3	−18.0±0.7	2060±180	209±2

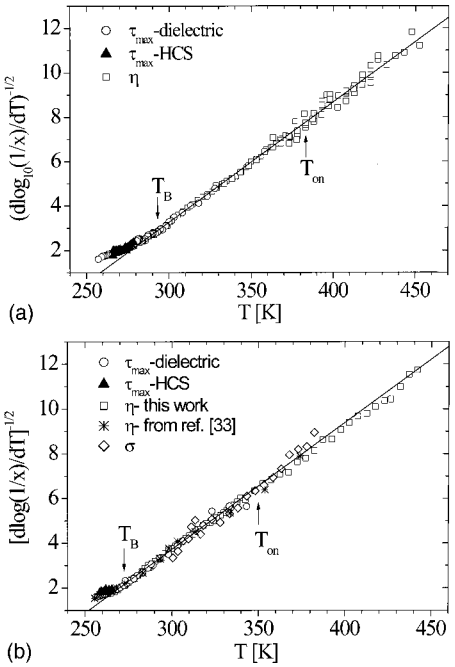

FIG. 9. Stickel plot (i.e., $[d\log_{10}(1/x)/dT]^{-1/2}$ vs T) for (a) PPGE and (b) DGEBA, obtained from $x=\tau_{\max}$, η, and σ. The symbols are explained in the legend. The straight line is a VFT fit to the high-temperature data. Arrows indicate the temperature of bending, T_B, and the temperature, T_{on}, where the dielectric α strength tends to zero.

In this formula, the isochoric specific heat c_v is approximated by the isobaric specific heat c_p, and $\Delta(1/c_p)$ is calculated as $\Delta(1/c_p)=1/c_{p,\text{glass}}-1/c_{p,\text{liquid}}$ with $c_{p,\text{glass}}$ and $c_{p,\text{liquid}}$ being the specific heat values for the glass and the liquid at the dynamic glass temperature T_ω from a tangent construction [Fig. 3(c)]. The average temperature fluctuation of a CRR, δT, is determined as the Gaussian dispersion of $c_p''(T)$.[55] M_0 is the molecular weight and R the molar gas constant. The temperature dependence of cooperativity as obtained from Eq. (3) is presented in Fig. 10. It should be noted that other approaches produce different expressions and yield significantly different estimates for the size of the CRR.[58,59]

IV. DISCUSSION

The above-reported results show that our epoxy resins have a rich relaxation map characterized by, at least, the main (a,α) transition and two secondary processes labeled β and γ. In this section two crossover regions will be recognized, somehow related to the β and γ processes and called β- and γ-crossover regions. The following discussion will also try to give an answer to the two questions (A) and (B) asked at the end of the Introduction, i.e., which of the crossover properties (ii)–(v) listed in the Introduction can be observed in the β- and γ-crossover region, and what is the character of that part of the main transition between the two crossovers. We will start with PPGE. The comparison with DGEBA and other systems with two secondary relaxations will be delegated to the last two subsections (E and F).

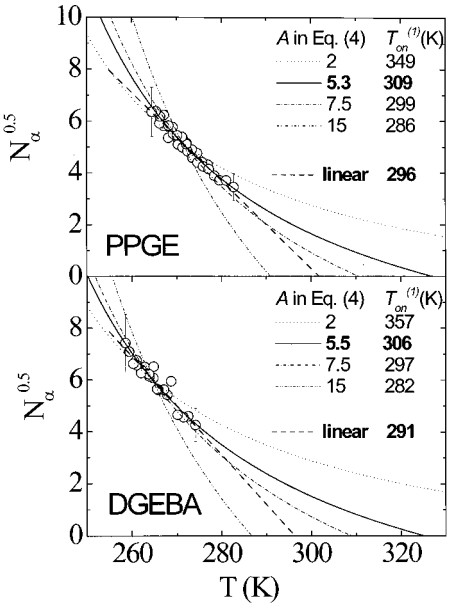

FIG. 10. Temperature-dependent cooperativity for PPGE and DGEBA. The lines are fits to the data using Eq. (4). The Vogel temperature (PPGE: $T_0 = 214$ K; DGEBA: $T_0 = 209$ K) was fixed and the A value was varied systematically to find the optimal fit (bold line) and the corresponding crossover temperature (PPGE: $A = 5.3$, $T_{on}^c = 327$ K, $T_{on}^{(1)} \sim 309$ K; DGEBA: $A = 5.5$, $T_{on}^c = 325$ K, $T_{on}^{(1)} \sim 306$ K). The thin lines are shown to give an impression of adjustments with different A values and their compatibility with data. Corresponding $T_{on}^{(1)}$ are given in the legend. The straight lines are linear fits to the data (PPGE: $T_{on}^{(1)} \sim 296$ K; DGEBA: $T_{on}^{(1)} \sim 291$ K). Typical errors are indicated.

A. γ-crossover region

Referring to the Arrhenius diagram and to the dielectric intensity $\Delta\varepsilon_\alpha$ for PPGE (Fig. 6), we find in the region where the relaxation times of main transition and γ relaxation approach each other, two properties that are typical of scenario I described in the Introduction, namely the onset of the α process with linearly increasing dielectric intensity [property (ii) of the Introduction] and the presence of a frequency gap in the Arrhenius plot between the extrapolated trace of the α process and the continuous trace of the a and γ processes. We refer to the region where the α intensity extrapolates to zero and the γ process continues into the a process of the main transition as the *γ-crossover region*. The onset extrapolation for $\Delta\varepsilon_\alpha$ is rather long, about 50 K, but the linear trend is well documented in a large temperature interval below 330 K. The onset of the α process is estimated at ($T_{on} = 391$ K, $\log_{10}(\omega_{on}[\text{rad/s}]) \approx 10$), see Table II, and the frequency gap to the extrapolated γ process at T_{on} is about $\Delta \log_{10}(\omega) \approx 1$ decade, with a large uncertainty. The extrapolation of the γ trace in the Arrhenius diagram (Fig. 11) above the glass transition temperature is complicated by two things: a significant curvature and a declining of the γ trace below the linear extrapolation from temperatures lower than T_g. We recall that both effects of the γ trace are not an artifact from the data evaluation since $\Delta\varepsilon_\gamma$ is large and the trace of the main transition in the Arrhenius diagram is two or more frequency decades below the measured γ trace.

Concerning $\Delta c_p(T)$ data from HCS, given in inset of Figs. 6(b) and 7(b) for comparison with dielectric data, they indicate a behavior similar to $\Delta\varepsilon_\alpha(T)$. Actually, we have no physical arguments for a linear extrapolation of Δc_p and, if any, such a large extrapolation does not give a reliable value for the temperature where $\Delta c_p \to 0$. Here we limit ourselves to note that the temperature behavior of Δc_p is consistent with going linearly to zero around the temperature T_{on} determined from dielectric data.

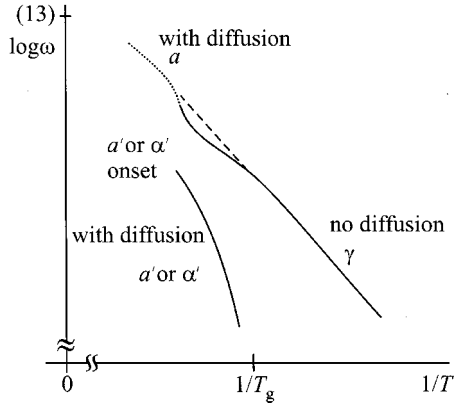

FIG. 11. Schematic sketch of the Arrhenius diagram near the γ-crossover region.

Unexpectedly, dielectric relaxation times and viscosity do not show any evidence of a Stickel bend [property (iii) of the Introduction] at the γ crossover (Fig. 9), i.e., the temperature dependence of dielectric relaxation time and viscosity does not reflect the change from the a trace to the α trace occurring with a one decade gap at T_{on}. No evidence is also given for a separation of the individual temperature dependences of different transport properties, such as electric conductivity and viscosity, and for an Adam–Gibbs bend[60] [properties (iv) and (v) of the Introduction].

B. β-crossover region

Referring again to the Arrhenius diagram and to the dielectric intensities in Fig. 6, we find now in the region where the relaxation times of main transition and β relaxation approach each other, two properties of scenario II: the continuous trace of the main transition and, second, the weak β relaxation, which runs into the main transition with a considerable ''angle'' in the Arrhenius diagram. We call this region the *β-crossover region*. The definition of a temperature where the separation of time scales between main and secondary relaxation occurs is not an unambiguous operation, since reflects the mentioned difficulty, in theory and practice, of analyzing the spectra in regions of strong overlap of the relaxation peaks. We refer to the $\alpha\beta$ splitting temperature T_β as the temperature where the linearly extrapolated Arrhenius behavior of τ_β intersects the α trace. In the extrapolation we obtain $T_\beta = 298$ K and $\log \omega_\beta(\text{rad/s}) = 6.2$ (Table II). Both the dielectric and the shear measurements of the main transition show a significant Stickel bend at the β crossover [property (iii), Fig. 9]. The Vogel temperatures are $T_0(T > T_\beta) = 240$ K and $T_0(T < T_\beta) = 214$ K, higher for the highest-temperature regime, in coincidence with the rule mentioned in the Introduction. There is an indication for start of separation of the individual temperature dependences of viscosity

TABLE IV. Comparison of γ-crossover and β-crossover properties for PPGE.

Property[a]	γ crossover	β crossover
Onset ($\Delta\varepsilon_\alpha \to 0$) of the low-temperature process (ii)	Yes	No
Frequency gap	Yes	No
Scenario	I	II
Stickel bend (iii)	No	Yes
Decoupling of η and σ (iv)	?	Yes
Adam–Gibbs bend (v)	?	Yes (Ref. 60)

[a]The roman numerals in parentheses are related to the properties (ii)–(v) of the Introduction.

and electric conductivity in the β-crossover region [property (iv), Fig. 8]. Calorimetric data published elsewhere[60] indicate a weak Adam–Gibbs bend in the same region [property (v); in Table II, T_{AG} is the temperature above which the deviation from the Adam–Gibbs relation, $\log \tau \propto (S_c T)^{-1}$, becomes appreciable]. The discussion of Secs. IV A and IV B is summarized in Table IV.

C. α process below the β crossover

For the discussion of the α process below the β crossover we use the experimental cooperativity $N_\alpha(T)$ obtained from the 3ω-method calorimetry (Fig. 10). A fair representation of its temperature dependence is usually[28,34,61]

$$N_\alpha^{1/2} = A(1-x)/x, \tag{4}$$

with x a reduced temperature between Vogel temperature ($x=0$) and a formal cooperativity-onset temperature ($x \to 1, N_\alpha^{1/2} \to 0$),

$$x = (T - T_0)/(T_{\text{on}}^c - T_0), \tag{5}$$

where A is a constant typically between 2 and 15,[61] T_0 the Vogel temperature, and T_{on}^c the cooperativity-onset temperature. For PPGE, Fig. 10 contains N_α data for temperatures between $T=264$ K and 283 K, and the β-crossover region is located around $T=298$ K. In extrapolating Eq. (4) to find the cooperativity-onset temperature we take the Vogel temperature T_0 from the VFT parameters for the low- temperature part of the α trace (Table II), $T_0=214$ K. Using Eq. (4), we obtain the best fit of the data of Fig. 10 for $A=5.3$ and $T_{\text{on}}^c = 327$ K. This gives a more realistic onset temperature corresponding to $N_\alpha=1$, $T(N_\alpha=1) \equiv T_{\text{on}}^{(1)} \sim 309$ K (Fig. 10). Considering the large uncertainty affecting $N_\alpha(\sim 30\%)$, a good fit of the data is still obtained with $A=7.5$, which gives $T_{\text{on}}^{(1)} \sim 299$ K. This value is not far from that which can be obtained from a linear extrapolation of the same data, giving $T_{\text{on}}^{(1)} \sim 296$ K. These temperature values indicate that the cooperativity-onset temperature $T_{\text{on}}^{(1)}$ for PPGE as defined by $N_\alpha \to 1$ is inside, or slightly above, the β-crossover region.[62]

D. Of which type is the main process between β and γ crossovers, a' or α'?

We come now to the question (B) asked at the end of the Introduction: What is the character of that part of the main transition between the two crossover regions? In general, for liquids of moderate molecular and structural complexity characterized by a single crossover region,[24,28] the main transition can be characterized as follows.

Above the crossover region we have the a process with the higher Vogel temperature when fitted by a VFT equation. In the molecular picture discussed in Ref. 24, the corresponding diffusion can be described as escaping of the particle from a cage[40] formed by the nearest neighbors. The cooperativity is of order $N_\alpha \sim 1$ when determined by Eq. (3) and decreases with higher temperatures. Such small cooperativities are unexpected and may be explained by an extraordinary concentration of free volume as generated by the Lévy distribution describing the escaping process. We may think about a ''cage door'' of size of about one particle temporarily opened by this concentration of free volume.[24]

Below the crossover region we have the α process with the lower Vogel temperature. The spatial aspect of its dynamic heterogeneity may be described[24] by an island of high mobility[63] assisted by a cooperativity shell of low mobility. The particle diffusion may be considered as generated by a diffusion of this island (Glarum defect diffusion[64]). This island of mobility may also be explained by an extraordinary concentration of free volume from a Lévy distribution. The spatial scale, however, is larger than that for the high-temperature a process and may generate sufficient free space for a secondary process at the island. In this molecular picture, the CRR as a representative subsystem for the main transition consists of two parts: the island of mobility and the cooperativity shell; the mobility contrast between these parts is responsible for the dynamic heterogeneity of the α process. The cooperativity is then the number of particles per CRR; it increases sharply with low temperatures and reaches values of order $N_\alpha \sim 100$ some 50 K below the crossover region.

Since we have two crossover regions in PPGE, the question arises whether the main process between the two crossovers is more an a process (in which case it will be called the a' process), because it is above the β crossover, or it is more an α process (in which case it will be called the α' process), because it is below the γ crossover. Reflecting the discussion in the previous subsections, Table IV, and the above criteria, we obtain the following indications.

In favor of an a' process, we have the small cooperativity $N_\alpha \sim 1$ obtained from the extrapolation at temperatures higher than the β crossover. This result is deduced upon the condition that there is no N_α increase with increasing temperature as observed for 19 systems studied so far by heat capacity spectroscopy[28] (apart from the indication of a weak $N_\alpha(T)$ irregularity in the β-crossover region of *ortho*-cresyl glycidyl ether[65]). Other arguments for an a' process are the location above a Stickel bend, above the start of a η-σ decoupling, and above a bend in the Adam–Gibbs plot.

In favor of an α' process, we have the occurrence at higher temperature of a dielectric onset with frequency gap, i.e., the location below a crossover region of the type described as scenario I.

Summarizing this subsection, we find more arguments suggesting that the main process between the β and γ crossovers is an a process (hence, a' process). Accordingly, we

should properly call the dielectric onset observed in the γ-crossover region the (a',α) onset. However, the intensity onset and frequency gap in the γ-crossover region indicate that there is, in PPGE, a qualitative difference between the a' process and the high-temperature a process, i.e., below and above the γ crossover. In particular, the presence of a frequency gap between the extrapolated a' and a processes at the γ crossover could be interpreted, following general scaling principles, as an indication of a length scale for the a' mode that is larger than that of the a modes emerging from the γ process.

E. Comparison between PPGE and DGEBA

The overall behavior of both epoxy resins is the same (Figs. 6, 7, 9, and 10): We find two crossover regions separated by a frequency difference of about four decades. The γ crossover seems to conform to scenario I (onset), the β crossover belongs to scenario II. The characteristic temperatures of crossover effects in DGEBA are compiled in Table II together with those for PPGE. Unlike PPGE, in DGEBA low-temperature conductivity data for assessing the presence of a σ-η bend (indicating the start of different temperature dependences for the different transport activities) are not available, and the weak bend of the dielectric γ-process intensity $\Delta\varepsilon_\gamma(T)$ at the β-crossover temperature is hardly perceived. From Fig. 10, the cooperativity of the α process, extrapolated to the β-crossover temperature, is about $N_\alpha \sim 5$ for DGEBA, i.e., a bit larger than that for PPGE. The extrapolation of $N_\alpha^{1/2}$ gives $N_\alpha = 1$ at $T_{\mathrm{on}}^{(1)} \sim 291$ K for the linear fit, and $T_{\mathrm{on}}^{(1)} \sim 306$ K for the best adjustment of Eq. (4) with $T_0 = 209$ K ($A = 5.5$ and $T_{\mathrm{on}}^{c} = 325$ K). The cooperativity N_α at the glass transition temperature, independently determined from DSC measurements is $N_\alpha(T_g) = 75 \pm 20$ for PPGE and $N_\alpha(T_g) = 110 \pm 30$ for DGEBA.[66] These values are consistent within the experimental errors with those extrapolated according to Eq. (4), and give comparable values for the cooperativity length ξ_α at the glass transition temperature for both PPGE and DGEBA [$\xi_\alpha(T_g) \cong 3.3 \pm 0.3$ and 3.8 ± 0.4 nm, respectively].

As recalled in Sec. III, the determination of T_0 as the temperature where the α trace tends to diverge is not unambiguous (in fact, it ranges from the values reported in Table III to values more than 10 K lower). It is worth noting that despite this large uncertainty the best adjustments of Eq. (4) with different values of T_0 do not entail changes in the extrapolated values of $T_{\mathrm{on}}^{(1)}$ and $N_\alpha(T_{\mathrm{g}})$ that are significant within the experimental errors.

Note that the frequency–temperature position of β and γ relaxations in PPGE and DGEBA are nearly identical (Table III). This indicates that the molecular mechanism of the secondary relaxations in both substances is similar. This aspect and the fact that there are two pronounced secondary processes in cross-linked DGEBA systems[67,68] may be the starting point of further studies on this topic.

F. Comparison with other substances

There are several substances with two secondary relaxations investigated in the literature.[69–75] However, only in a very few of these samples do both secondary relaxations approach the main transition inside the experimentally accessible frequency window below 10 GHz and is information about dielectric strengths available. We will discuss below a few previously investigated samples and compare their behavior with our epoxy resins.

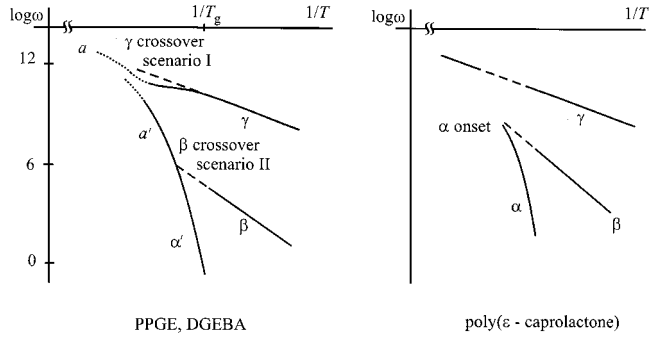

FIG. 12. Comparison of the Arrhenius diagrams for the epoxy resins (this paper) and poly(ε-caprolactone) from literature (Ref. 73) (schematically).

Schematic Arrhenius diagrams for poly(ε-caprolactone) from Fig. 9 of Ref. 73 and for our epoxy resins (Figs. 6 and 7) show significant differences (Fig. 12). For poly(ε-caprolactone) the dielectric α onset coincides with the $\alpha\beta$ merging, and the frequency gap to the continuous γ process is about two decades. We may imagine, purely phenomenologically, that the poly(ε-caprolactone) scenario would emerge from our epoxy resin situation when the γ-process frequency near the onset is about two frequency decades lower. Then the two crossover regions of the epoxy resins would coincide and the a' process between the two crossovers would disappear. For poly(ε-caprolactone) the γ process deviates less from the linear extrapolation, but a small sigmoidal shape of the γ trace in the Arrhenius diagram seems also to occur. As a whole, it seems that the difference between the two diagrams in Fig. 12 is caused by the difference in the crossover frequency.

A comparison of our data for PPGE and DGEBA with those for another epoxy resin with two secondary relaxations, *ortho*-cresyl glycidyl ether[65] also indicates differences. There is no dielectric α onset in the γ-crossover region, but the β as well as γ crossover is accompanied by a Stickel bend, i.e., a change in the temperature dependence of the main relaxation time. In contrast, the data for triphenylolmethane triglycidyl ether[74] indicate, as far as data are available in the temperature range below $1.22T_g$, many similarities with the features of PPGE and DGEBA.

Another class of substances with two secondary relaxations are the poly(*n*-alkyl methacrylate)s. Due to the high frequency of the γ relaxation in samples with high molecular weight, less is known about the details of a possible γ crossover. However, for short poly(*n*-butyl methacrylate) oligomers the γ-relaxation intensity increases with decreasing chain length.[75,76] This is also reflected by an increase of the calorimetric α intensity and the cooperativity near T_g, indicating relations between local γ dynamics and main transition besides those in the well-investigated β-crossover region.[7,22,43]

V. CONCLUSIONS

The dynamic glass transition of PPGE and DGEBA has been studied by means of broadband dielectric spectroscopy, heat capacity spectroscopy (3ω method), and viscosimetry. Two well-separated crossover regions (β crossover and γ crossover) have been identified, around $T_c(\beta)\sim(1.1-1.2)T_g$, $\tau_c(\beta)\approx 10^{-6}$ s, and $T_c(\gamma)\sim(1.4-1.5)T_g$, $\tau_c(\gamma)\approx 10^{-10}$ s, respectively.

The γ crossover is characterized by the onset of the (a',α) transition, with a relaxation time about one decade greater than that of the continuous trace of the (a,γ) processes, the a process being the high-temperature part of the main dynamic transition. In the intermediate-temperature region, between the γ and β crossover, the main transition seems to be characterized by a low cooperativity $N_\alpha\sim 1$, and it has been labeled a' for analogies with the high-temperature a process. At lower temperatures, the β crossover is characterized by a continuous trace of the main (a',α) transition where the crossover region is identified by the extrapolation from lower temperatures of the β relaxation time to the main relaxation time; a Stickel bend in the trace of the (a',α) transition with a Vogel temperature T_0 for the α process which is smaller than that for the a' process; and the separation of the individual temperature dependences of different transport properties such as impurity-ion diffusion coefficient and viscosity (*breakdown* of the Stokes–Einstein law). The comparison of dielectric relaxation times with configurational entropy data from calorimetry shows the validity of the Adam–Gibbs relation for the temperature dependence of the α relaxation time at temperatures below the β-crossover region.[60] There, cooperativity starts to increase significantly.

Also the secondary relaxations show changes across the glass transitions. A significant curvature and a lowering of the γ trace below the linear extrapolation from temperatures lower than T_g can be clearly observed in the Arrhenius plot of both PPGE and DGEBA. These effects are not an artifact of the data evaluation since $\Delta\varepsilon_\gamma$ is large enough and the trace of the main transition in the Arrhenius plot is two or more frequency decades below the measured γ trace. Another interesting feature shown by secondary processes is the influence of freezing-in on the amplitude of the γ relaxation $\Delta\varepsilon_\gamma(T)$, which shows a significant bend at T_g. This suggests the existence of some intrinsic relation between the dynamic glass transition and secondary relaxations. Temperature effects on secondary relaxations promise to be important for a deeper understanding of the glass transition phenomenon and are currently the subject of further theoretical and experimental effort.

ACKNOWLEDGEMENTS

We thank P. A. Rolla and M. Lucchesi for helpful discussions, and acknowledge financial support from MIUR-PRIN2000, the Deutsche Forschungsgemeinschaft DFG (in particular, S.C. acknowledges the SFB 418 supporting her stay in Halle) and the Fonds Chemische Industrie FCI.

[1] M. Beiner, H. Huth, and K. Schröter, J. Non-Cryst. Solids **279**, 126 (2001).
[2] K. L. Ngai, J. Non-Cryst. Solids **275**, 7 (2000).
[3] G. Williams, Trans. Faraday Soc. **62**, 2091 (1966).
[4] G. P. Johari and M. Goldstein, J. Chem. Phys. **53**, 2372 (1970).
[5] G. P. Johari and M. Goldstein, J. Chem. Phys. **55**, 4245 (1971).
[6] G. P. Johari and M. Goldstein, J. Chem. Phys. **74**, 2034 (1970).
[7] F. Garwe, A. Schönhals, H. Lockwenz, M. Beiner, K. Schröter, and E. Donth, Macromolecules **29**, 247 (1996).
[8] R. Casalini, D. Fioretto, A. Livi, M. Lucchesi, and P. A. Rolla, Phys. Rev. B **56**, 3016 (1997).
[9] S. Kahle, J. Korus, E. Hempel, R. Unger, S. Höring, K. Schröter, and E. Donth, Macromolecules **30**, 7214 (1997).
[10] F. Stickel, PhD thesis, Universität Mainz, Mainz, Germany, 1995.
[11] F. Stickel, E. W. Fischer, and R. Richert, J. Chem. Phys. **102**, 6251 (1995).
[12] F. Stickel, E. W. Fischer, and R. Richert, J. Chem. Phys. **104**, 2043 (1996).
[13] C. Hansen, F. Stickel, R. Richert, and E. W. Fischer, J. Chem. Phys. **108**, 6408 (1998).
[14] F. Fujara, B. Geil, H. Sillescu, and G. Fleischer, Z. Phys. B: Condens. Matter **88**, 195 (1992).
[15] J. H. Magill and D. J. Plazek, J. Chem. Phys. **46**, 3757 (1967).
[16] K. L. Ngai, J. H. Magill, and D. J. Plazek, J. Chem. Phys. **112**, 1887 (2000).
[17] E. Rössler, Phys. Rev. Lett. **65**, 1595 (1990).
[18] G. Adam and J. H. Gibbs, J. Chem. Phys. **43**, 139 (1965).
[19] R. Richert and C. A. Angell, J. Chem. Phys. **108**, 9016 (1998).
[20] K. Ngai, Phys. Rev. E **57**, 7346 (1998).
[21] K. L. Ngai, J. Chem. Phys. **111**, 3639 (1999).
[22] M. Beiner, S. Kahle, E. Hempel, K. Schröter, and E. Donth, Europhys. Lett. **44**, 321 (1998).
[23] S. Kahle, K. Schröter, E. Hempel, and E. Donth, J. Chem. Phys. **111**, 6462 (1999).
[24] E. Donth, *The Glass Transition. Relaxation Dynamics in Liquids and Disordered Materials* (Springer, Berlin 2001).
[25] S. S. N. Murthy, J. Chem. Soc., Faraday Trans. 2 **85**, 581 (1989).
[26] S. S. N. Murthy, J. Mol. Liq. **44**, 51 (1989).
[27] A. Schönhals, in *Non Equilibrium Phenomena in Supercooled Fluids, Glasses and Amorphous Materials*, edited by M. Giordano, D. Leporini, and M. Tosi (World Scientific, Singapore 1996), p. 210.
[28] E. Donth, H. Huth, and M. Beiner, J. Phys.: Condens. Matter **13**, L451 (2001).
[29] S. Corezzi, S. Capaccioli, R. Casalini, D. Fioretto, M. Paluch, and P. A. Rolla, Chem. Phys. Lett. **320**, 113 (2000).
[30] W. H. Press, S. A. Teukolsky, W. T. Vetterling, and B. P. Flannery, *Numerical Recipes* (Cambridge University Press, Cambridge, 1992).
[31] N. O. Birge and S. R. Nagel, Phys. Rev. Lett. **54**, 2674 (1985).
[32] J. Korus, M. Beiner, K. Busse, S. Kahle, R. Unger, and E. Donth, Thermochim. Acta **304/305**, 99 (1997).
[33] H. Huth, M. Beiner, S. Weyer, M. Merzlyakov, C. Schick, and E. Donth, Thermochim. Acta **377**, 113 (2001).
[34] H. Huth, M. Beiner, and E. Donth, Phys. Rev. B **61**, 15092 (2000).
[35] K. Schröter and E. Donth, J. Chem. Phys. **113**, 9101 (2000).
[36] L. Comez, D. Fioretto, L. Palmieri *et al.*, Phys. Rev. E **60**, 3086 (1999).
[37] M. Beiner, J. Korus, H. Lockwenz, K. Schröter, and E. Donth, Macromolecules **29**, 5183 (1996).
[38] P. K. Dixon and S. R. Nagel, Phys. Rev. Lett. **61**, 341 (1988).
[39] P. K. Dixon, Phys. Rev. B **42**, 8179 (1990).
[40] W. Götze and L. Sjögren, Rep. Prog. Phys. **55**, 241 (1992).
[41] F. Alvarez, A. Hoffman, A. Alegría, and J. Colmenero, J. Chem. Phys. **105**, 432 (1996).
[42] A. Arbe, D. Richter, J. Colmenero, and B. Farago, Phys. Rev. E **54**, 3853 (1996).
[43] K. Schröter, R. Unger, S. Reissig, F. Garwe, S. Kahle, M. Beiner, and E. Donth, Macromolecules **31**, 8966 (1998).
[44] R. Bergman, F. Alvarez, A. Alegría, and J. Colmenero, J. Chem. Phys. **109**, 7546 (1998).
[45] E. Donth, K. Schröter, and S. Kahle, Phys. Rev. E **60**, 1099 (1999).
[46] A. Arbe, J. Colmenero, D. Gómez, D. Richter, and B. Farago, Phys. Rev. E **60**, 1103 (1999).
[47] A. Kudlik, S. Benkhof, T. Blochowicz, C. Tschirwitz, and E. Rössler, J. Mol. Struct. **479**, 201 (1999).
[48] A. Justl, Degree thesis, Universität Bayreuth, Bayreuth, Germany, 2000.
[49] S. Capaccioli (unpublished).
[50] S. Corezzi, E. Campani, P. A. Rolla, S. Capaccioli, and D. Fioretto, J.

Chem. Phys. **111**, 9343 (1999). In that work we called β relaxation what is labeled here γ relaxation.
[51] H. Z. Cummins, J. Hernandez, W. M. Du, and G. Li, Phys. Rev. Lett. **73**, 2935 (1994).
[52] A. Schönhals, F. Kremer, A. Hofmann, E. W. Fischer, and E. Schlosser, Phys. Rev. Lett. **70**, 3459 (1993).
[53] For a discussion of the problems involved in assessing data fitting, see C. A. Angell, K. L. Ngai, G. B. McKenna, P. F. McMillan, and S. W. Martin, J. Appl. Phys. **88**, 3113 (2000).
[54] E. Donth, J. Non-Cryst. Solids **53**, 325 (1982).
[55] E. Hempel, G. Hempel, A. Hensel, C. Schick, and E. Donth, J. Phys. Chem. B **104**, 2460 (2000) (see Appendix).
[56] E. Donth, *Relaxation and Thermodynamics in Polymers. Glass Transition* (Akademie, Berlin 1992).
[57] M. von Laue, Phys. Z. **18**, 542 (1917).
[58] H. Sillescu, J. Non-Cryst. Solids **243**, 81 (1999).
[59] O. Yamamuro, I. Tsukushi, A. Lindqvist, S. Takahara, M. Ishikawa, and T. Matsuo, J. Phys. Chem. B **102**, 1605 (1998).
[60] S. Corezzi, D. Fioretto, S. C. Santucci, S. Capaccioli, R. Casalini, M. Lucchesi, E. Hempel, and M. Beiner, Philos. Mag. B **82**, 339 (2002).
[61] J. Korus, E. Hempel, M. Beiner, S. Kahle, and E. Donth, Acta Polym. **48**, 369 (1997).
[62] This finding is consistent with the change of Vogel temperatures in the β-crossover region, mentioned above. Interpreting $k_B T_0$ as a measure of the roughness for the relevant energy landscape (Refs. 21 and 51), we see that the landscape for the α process has a lower roughness than those of the a' or α' process. (see Sec. IV D) above the β-crossover region. Increasing the cooperativity permits the phase-space point of representative subsystems to find its way through the landscape with low "saddles" accessible also at low temperature. Above the β crossover, at higher temperatures, the system can do with higher landscape saddles and does not need the cooperativity with rare low saddles.
[63] G. P. Johari and E. Whalley, Faraday Symp. Chem. Soc. **6**, 23 (1972).
[64] S. H. Glarum, J. Chem. Phys. **33**, 639 (1960).
[65] H. Huth, PhD thesis, Universität Halle, Halle, Germany, 2001.
[66] E. Hempel (unpublished).
[67] I. Alig and G. P. Johari, J. Polym. Sci., Polym. Phys. Ed. **31**, 299 (1993).
[68] M. Beiner and G. P. Johari (unpublished).
[69] N. G. McCrum, B. E. Read, and G. Williams, *Anelastic and Dielectric Effects in Polymeric Solids* (Wiley, London 1967).
[70] R. Greus, G. Ribellez, and D. Calleja, Polymer **26**, 1849 (1985).
[71] Gangasharan and S. S. N. Murthy, J. Chem. Phys. **99**, 9865 (1993).
[72] T. Nicolai and G. Floudas, Macromolecules **31**, 2578 (1998).
[73] M. Grimau, E. Laredo, Y. M. C. Perez, and A. Bello, J. Chem. Phys. **114**, 6417 (2001).
[74] D. Pisignano, S. Capaccioli, R. Casalini, M. Lucchesi, P. A. Rolla, A. Justl, and E. Rössler, J. Phys.: Condens. Matter **13**, 4405 (2001).
[75] M. Beiner, Macromol. Rapid Commun. **22**, 869 (2001).
[76] S. Reissig, PhD thesis, Universität Halle, Halle, Germany, 2000.